



# MIT Open Access Articles

## *A 2.5-GHz asymmetric multilevel outphasing power amplifier in 65-nm CMOS*

The MIT Faculty has made this article openly available. **Please share** how this access benefits you. Your story matters.

<b>Citation</b>	Godoy, Philip A., SungWon Chung, Taylor W. Barton, David J. Perreault, and Joel L. Dawson. "A 2.5-GHz Asymmetric Multilevel Outphasing Power Amplifier in 65-Nm CMOS." 2011 IEEE Topical Conference on Power Amplifiers for Wireless and Radio Applications (n.d.).
<b>As Published</b>	<a href="http://dx.doi.org/10.1109/PAWR.2011.5725372">http://dx.doi.org/10.1109/PAWR.2011.5725372</a>
<b>Publisher</b>	Institute of Electrical and Electronics Engineers (IEEE)
<b>Version</b>	Author's final manuscript
<b>Citable link</b>	<a href="http://hdl.handle.net/1721.1/86974">http://hdl.handle.net/1721.1/86974</a>
<b>Terms of Use</b>	Creative Commons Attribution-Noncommercial-Share Alike
<b>Detailed Terms</b>	<a href="http://creativecommons.org/licenses/by-nc-sa/4.0/">http://creativecommons.org/licenses/by-nc-sa/4.0/</a>

# A 2.5-GHz Asymmetric Multilevel Outphasing Power Amplifier in 65-nm CMOS

Philip A. Godoy, SungWon Chung, Taylor W. Barton, David J. Perreault, and Joel L. Dawson

Massachusetts Institute of Technology, Cambridge, MA, 02139, USA

**Abstract**—We present a high-efficiency transmitter based on asymmetric multilevel outphasing (AMO). AMO transmitters improve their efficiency over LINC (linear amplification using nonlinear components) transmitters by switching the output envelopes of the power amplifiers among a discrete set of levels. This minimizes the occurrence of large outphasing angles, reducing the energy lost in the power combiner. We demonstrate this concept with a 2.5-GHz, 20-dBm peak output power transmitter using 2-level AMO designed in a 65-nm CMOS process. To the authors' knowledge, this IC is the first integrated implementation of the AMO concept. At peak output power, the measured power-added efficiency is 27.8%. For a 16-QAM signal with 6.1dB peak-to-average power ratio, the AMO prototype improves the average efficiency from 4.7% to 10.0% compared to the standard LINC system.

**Index Terms**—power amplifier (PA), outphasing, LINC, asymmetric power combining, asymmetric multilevel outphasing (AMO), digital predistortion

## I. INTRODUCTION

Wideband RF power amplifiers (PAs) with high efficiency are of great importance in high-data-rate communications. Tremendous efforts to beat the linearity-efficiency tradeoff for PAs have led to a wide variety of architectures, including polar, outphasing, envelope tracking, feedforward, Cartesian feedback, predistortion, Doherty, RF pulse width modulation, and RF delta-sigma modulation [1].

Outphasing architectures [2], [3] are capable of transmitting very wideband signals and are thus suitable for wideband communication in multi-standard applications. However, outphasing power efficiency is poor at large power back-off, a critical drawback for wideband signals with high peak-to-average power ratio (PAPR). Outphasing with lossless nonlinear power combining [4], [5] improves efficiency at the cost of reduced linearity and bandwidth.

Recently, asymmetric multilevel outphasing (AMO) has been proposed for high-efficiency wideband RF transmission [6], [7], [8]. This paper presents the first IC implementation of this technique. AMO improves the classical outphasing power efficiency by switching the output amplitudes of the PAs among a discrete set of levels. In this work, the discrete amplitude changes are accomplished by switching the supply voltages of the PAs. This discrete amplitude modulation reduces the amount of outphasing required, thereby reducing the power lost in the combiner. A block diagram of the AMO system with supply voltage switching is shown in Fig. 1.

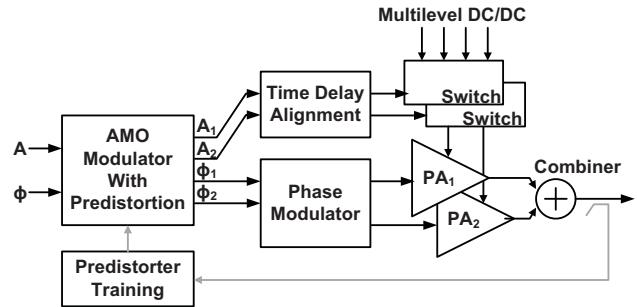


Fig. 1. Asymmetric multilevel outphasing (AMO) transmitter with supply voltage switching.

## II. AMO SYSTEM

### A. AMO Modulation

Fundamentally, AMO modulation decomposes a complex vector, which represents a baseband constellation point, into two vectors such that the sum of the two vectors constructs the original complex vector with the *minimum* outphasing angle, as illustrated in Fig. 2(a). The minimum outphasing angle is desirable because it minimizes the loss in an isolating power combiner. In Fig. 2(a), the two vectors are the baseband representation of the two PA outputs. Compared to multilevel LINC (ML-LINC) [9], by making independent changes in the output amplitude for each of the two outphased PAs, the AMO technique results in smaller outphasing angles so that higher efficiency can be achieved. The efficiency of LINC, ML-LINC, and AMO are compared in Fig. 3.

Mathematically, AMO modulation for a polar constellation point  $\{A(t), \phi(t)\}$  can be formulated using the law of cosines:

$$\begin{aligned}\phi_1(t) &= \phi(t) + \cos^{-1} \frac{(V_1(t)^2 + A(t)^2 - V_2(t)^2)}{2V_1(t)A(t)}, \\ \phi_2(t) &= \phi(t) - \cos^{-1} \frac{(V_2(t)^2 + A(t)^2 - V_1(t)^2)}{2V_2(t)A(t)}\end{aligned}\quad (1)$$

where  $V_1(t)$  and  $V_2(t)$  are the output voltages of the two PAs and  $\phi_1(t)$  and  $\phi_2(t)$  are the phases of the two PAs in outphasing (see Fig. 2(b) for notational convention). When assigning  $V_1(t)$ ,  $V_2(t)$ ,  $\phi_1(t)$  and  $\phi_2(t)$  to the two

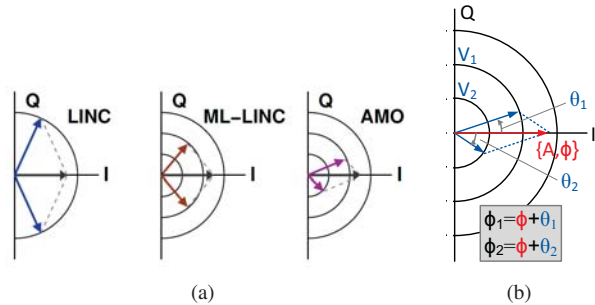


Fig. 2. (a) Signal component vector diagram for LINC, ML-LINC, and AMO. The smallest outphasing angle is achieved with AMO. (b) Notational convention.

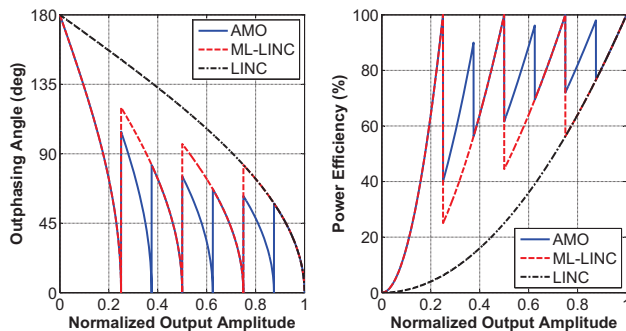


Fig. 3. Outphasing angle and power efficiency of AMO modulation compared to LINC and ML-LINC.

PAs, multiple solutions exist. The solution that minimizes the loss in the isolating combiner should be chosen.

Loss in an isolating combiner, such as a Wilkinson, results when the inputs are driven out of phase and/or driven with unequal amplitudes. The efficiency of the combiner is given by the following equation:

$$\eta_c = \frac{(V_1 \cos \theta_1 + V_2 \cos \theta_2)^2}{2(V_1^2 + V_2^2)}. \quad (2)$$

Because the AMO architecture allows the two PA amplitudes to be unequal, there can also be loss in the combiner even when there is no outphasing.

In an AMO system, if there are  $N$  different PA output amplitudes  $V_1$  to  $V_N$ , there are  $\binom{N}{2} + N$  combinations of amplitudes for the two PAs. However, as can be seen in Eq. 2, the combiner efficiency decreases as the difference between two amplitudes increases. Therefore, in our system we restrict the combinations to be adjacent amplitude levels (i.e.,  $V_k$  and  $V_{k+1}$ ).

### B. Multi-standard Efficiency Optimization

For a given modulated signal's probability density function (PDF), we can choose the values of the PA output amplitudes  $V_k$  such that the efficiency of the AMO system is maximized. In this way, we can optimize the AMO system for multiple wireless communication standards. For

the AMO system that uses supply voltage switching, this is accomplished simply by changing the supply voltages. The optimum values can be determined as follows.

Let us define the output amplitude levels  $r_k$  to be the maximum output amplitudes for each of the different supply voltage levels  $V_{sup,k}$  when both PAs are driven by the same supply. Let us also define  $\eta_{pa}(r_k)$  to be the PA efficiency when the output amplitude is  $r_k$ . The total average efficiency can be computed as

$$\eta_{avg} = \frac{\langle P_{out} \rangle}{\langle P_{DC} \rangle} \quad (3)$$

If the amplitude PDF  $p(A)$  of the transmitted signal is known, then the average output power is simply

$$\langle P_{out} \rangle = \int p(A) A^2 dA \quad (4)$$

To determine the average DC power, we divide the PDF into several regions separated by the  $r_k$  (and their combinations), and for each region we integrate the PDF curve to find the total probability in that region and multiply that probability by the DC power consumption when the AMO system operates in that region. With the combinations of supply voltages restricted to be adjacent supply levels, the average DC power can be computed as

$$\begin{aligned} \langle P_{DC} \rangle &= \frac{r_1^2}{\eta_{pa}(r_1)} \int_0^{r_1} p(A) dA \\ &+ \sum_{k=1}^{N-1} \left[ \frac{1}{2} \left( \frac{r_k^2}{\eta_{pa}(r_k)} + \frac{r_{k+1}^2}{\eta_{pa}(r_{k+1})} \right) \int_{r_k}^{\frac{r_k+r_{k+1}}{2}} p(A) dA \right. \\ &\quad \left. + \frac{r_{k+1}^2}{\eta_{pa}(r_{k+1})} \int_{\frac{r_k+r_{k+1}}{2}}^{r_{k+1}} p(A) dA \right] \end{aligned} \quad (5)$$

Using this equation, the optimum set of supply voltage levels for a given amplitude PDF can be found by first measuring the PA efficiency  $\eta_{pa}(r_k)$  as a function of  $r_k$  (sweeping the supply voltage), and then performing an exhaustive search on the  $N$  values of the  $r_k$ .

### III. AMO PROTOTYPE

To demonstrate the feasibility of the AMO system, a prototype was designed and implemented in a 65-nm CMOS process at a carrier frequency of 2.5 GHz. Fig. 4 shows the circuit schematic of the PA used in the AMO prototype. The PAs operate in class E and utilize a thick-oxide cascode transistor to reduce voltage stress on the main switch. The output network consists of the shunt capacitance from the cascode device and a spiral inductor for the DC feed. It should be noted that the fabricated chip does not have an ultra-thick metal layer, limiting the quality factor of the on-chip inductors. The matching network and series resonant filter necessary for class-E operation are implemented with bondwire inductance and off-chip discrete-component capacitors.

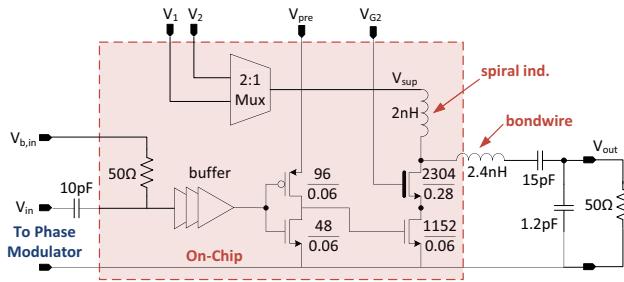


Fig. 4. Circuit schematic of the class-E PA used in the AMO prototype. The single-ended version is shown for simplicity.

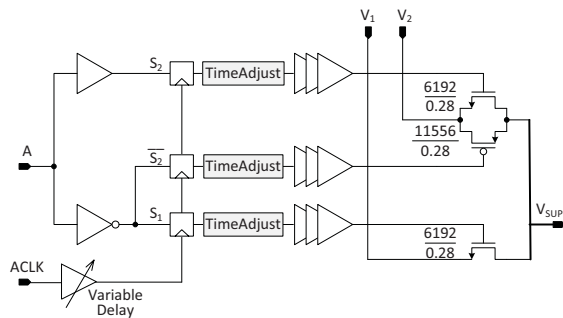


Fig. 5. Circuit schematic of the PA supply modulator.

Fig. 5 shows the circuit schematic of the PA supply modulator. The chip can switch between 2 different supply voltages, which come from off-chip regulators. The power supply switches are designed for small on-resistance compared to the load impedance presented to the PAs. The higher supply switch has an additional PMOS device to pass higher voltages. A time adjustment circuit is included for each switch control signal to change the timing of the signal transitions for time alignment purposes. The switch select signals are clocked for synchronization, and the clock signal has a variable delay to perform time alignment between the amplitude and phase paths.

The die photo is shown in Fig. 6. The area of the PAs and the supply modulator is 1.2x1.2mm<sup>2</sup>.

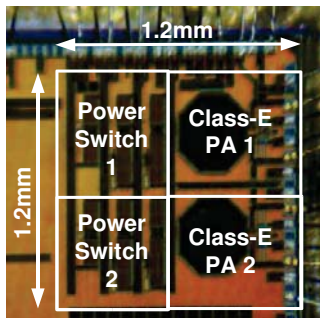


Fig. 6. Die photo of the AMO prototype.

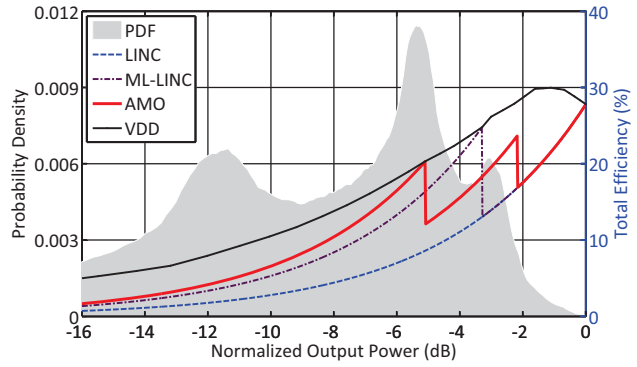


Fig. 7. Measured PAE vs. output power for the AMO prototype, along with the optimized amplitude levels for a 16-QAM signal with 6.1dB PAPR. The PDF of the 16-QAM signal is also shown.

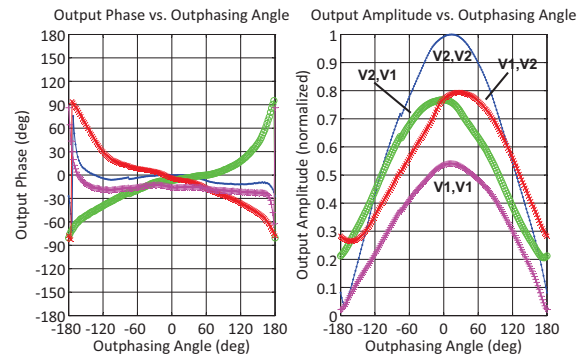


Fig. 8. Measured output amplitude and phase distortion for the AMO prototype. Each curve corresponds to a different combination of supply voltages for the two outphased PAs.

#### IV. MEASUREMENT RESULTS

Fig. 7 shows the measured power-added efficiency (PAE) vs. output power for the prototype transmitter at 2.5 GHz as the supply voltage to both PAs is varied. For a given number of supply voltage levels, this data can be used to find the optimum amplitude values that maximize the efficiency for a given probability density function (PDF). In this work we use 2 supply voltage levels, and we tested our system with a 5-Msym/s 16-QAM signal with a PAPR of 6.1dB. The corresponding optimum efficiency curves for the AMO prototype are shown in Fig. 7. It can be seen that the AMO system provides a significant efficiency improvement over standard LINC.

Fig. 8 shows the measured amplitude and phase of the output voltage at the fundamental of the RF output frequency vs. the outphasing angle. The phase measurements are normalized to the output phase at the maximum output power. There are 4 different curves, each for a different combination of supply voltage levels for the 2 outphased PAs. A lookup table (LUT) constructed from the data in Fig. 8 is used to correct for the static nonlinearity.

To demonstrate the linearity of the system, we tested

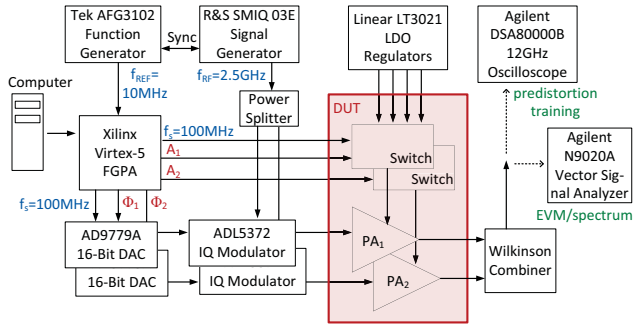


Fig. 9. System testbench for the AMO prototype.

the prototype with a 5-Msym/s 16-QAM signal with a PAPR of 6.1dB. The testbench is shown in Fig. 9. The digital baseband data generation and associated signal processing were performed in MATLAB and uploaded into the internal RAM of an FPGA. The baseband amplitude data was fed from the FPGA to the PA supply modulator shown in Fig. 5. To implement the phase modulators, the baseband phase data was fed from the FPGA into the inputs of two 16-bit I/Q DACs, each followed by a quadrature modulator to upconvert the baseband data to the RF carrier frequency of 2.5 GHz. The two RF signals were then fed to the two PAs in the AMO prototype IC as shown in Fig. 4. The FPGA sampling rate was 100 MHz.

Fig. 10 shows the measured demodulated 16-QAM constellation and spectrum from the AMO PA after predistortion. With 13-dBm output power, the AMO PA achieves a measured EVM of 2.5%-rms. For reference, the measured EVM for the standard LINC case is 2.3%-rms. Fig. 11 compares the measured output spectrum of the prototype for the standard LINC case and for the AMO system. We see that the noise floor is slightly higher for the AMO system compared to that of the LINC system. Our experiments and simulation indicate that this is due to the abrupt amplitude and phase changes that occur when the PA supply voltages are switched, together with insufficient timing alignment between the amplitude and phase paths as well as the finite bandwidth of the phase modulators. In a planned revision, we intend to improve performance by increasing the range and resolution of the time alignment system implemented on the chip and using a higher speed phase modulator. The AMO system improves the overall efficiency from 4.7% to 10.0% compared to the standard LINC system, an efficiency improvement of more than 2x.

## V. CONCLUSION

In this paper, we have presented the first IC implementation of the AMO concept. The AMO modulation technique was described, along with the optimization procedure for the discrete amplitude levels based on the envelope distribution of the modulated signal. A prototype IC was fabricated in a 65-nm CMOS process, operating

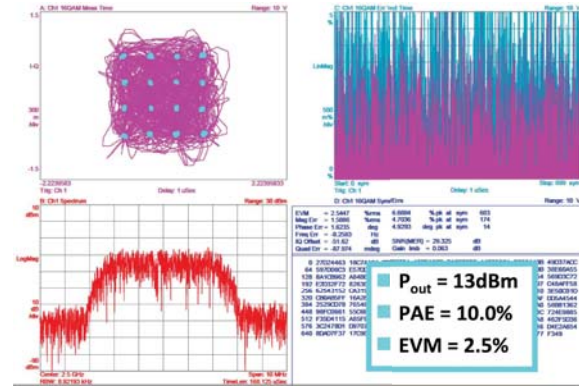


Fig. 10. Measured EVM and spectrum of the 5-Msym/s 16-QAM transmission for the AMO prototype after predistortion.

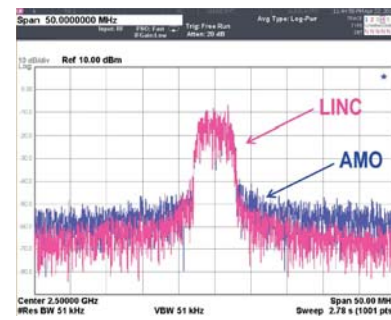


Fig. 11. Measured transmit spectrum of the 16-QAM signal.

at a carrier frequency of 2.5 GHz and delivering 20-dBm peak power with 27.8% PAE. The prototype was tested with a 5-Msym/s 16-QAM signal with a PAPR of 6.1dB and improves the overall efficiency from 4.7% to 10.0% compared to the standard LINC system.

## ACKNOWLEDGMENT

The authors wish to acknowledge the TSMC University Shuttle Program for the fabrication of this design.

## REFERENCES

- [1] F. H. Raab, "Power amplifiers and transmitters for RF and microwave," *IEEE Trans. Microwave Theory Tech.*, vol. 50, no. 3, pp. 814–826, Mar. 2002.
- [2] H. Chireix, "High-power outphasing modulation," *Proc. of the IRE*, vol. 23, pp. 1370–1392, 1935.
- [3] D. C. Cox, "Linear amplification with nonlinear components," *IEEE Trans. Commun.*, pp. 1942–1945, Dec. 1974.
- [4] S. Moloudi *et al.*, "An outphasing power amplifier for a software-defined radio transmitter," in *ISSCC*, 2008, pp. 568–569.
- [5] R. Beltran *et al.*, "HF outphasing transmitter using class-E power amplifiers," in *IEEE Int'l Microwave Symp.*, 2009, pp. 757–760.
- [6] S. Chung *et al.*, "Asymmetric multilevel outphasing architecture for multistandard transmitters," in *IEEE RFIC Symp.*, 2009, pp. 237–240.
- [7] J. Hur *et al.*, "Highly efficient uneven multi-level LINC transmitter," *Electronic Letters*, pp. 837–838, July 2009.
- [8] S. Chung *et al.*, "Asymmetric multilevel outphasing transmitter using class-E PAs with discrete pulse width modulation," in *IEEE Int'l Microwave Symp.*, 2010, pp. 264–267.
- [9] Y.-J. Chen *et al.*, "Multilevel LINC system design for wireless transmitters," in *Int'l Symp. on VLSI-DAT*, 2007.